





Interaction of low-energy muons with defect profiles in proton-irradiated Si and 4H-SiC

Judith Woerle ^{1,2,*}, Thomas Prokscha ³, Anders Hallén ⁴, and Ulrike Grossner ¹

¹Advanced Power Semiconductor Laboratory, ETH Zurich, 8092 Zurich, Switzerland

²Laboratory for Micro- and Nanotechnology, Paul Scherrer Institute, 5232 Villigen, Switzerland

³Laboratory for Muon Spin Spectroscopy, Paul Scherrer Institute, 5232 Villigen, Switzerland

⁴Royal Institute of Technology, KTH-ICT, Electrum 229, SE-164 40 Stockholm, Sweden



(Received 31 July 2019; published 17 September 2019)

Muon spin rotation (μ SR) with low-energy muons is a powerful nuclear method where electrical and magnetic properties of thin films can be investigated in a depth-resolved manner. Here, we present a study on proton-irradiated Si and 4H-SiC where the formation of the hydrogen-like muonium (Mu) is analyzed as a function of the proton dose. While the Mu formation is strongly suppressed in the highly defective region of the shallow proton stopping profile, the Mu signal quickly recovers for higher muon energies where the muons reach the untreated semiconductor bulk. A lower sensitivity limit of low-energy μ SR to crystal defects of around 10^{17} to 10^{18} cm^{-3} is estimated. Our results demonstrate the high potential of this technique to nondestructively probe near-surface regions without the need for electronic device fabrication and to provide valuable complementary information when investigating defects in semiconductors.

DOI: [10.1103/PhysRevB.100.115202](https://doi.org/10.1103/PhysRevB.100.115202)

I. INTRODUCTION

The muon spin rotation spectroscopy technique (μ SR) usually uses positive muons as a local magnetic probe to investigate electronic and magnetic properties of materials. Nearly 100% spin-polarized beams of typically MeV energies are implanted in matter, where the muons rapidly thermalize (≈ 10 ps) without loss of polarization. The muon is an unstable elementary particle with a lifetime of $2.2\mu\text{s}$. The evolution of the muon spin polarization can be measured by detecting the anisotropically emitted decay positrons, from which local information about electronic and magnetic properties is obtained.

In metals, the positive charge of the muon is collectively screened by a cloud of conduction electrons and the muon spin precesses like a free muon at its Larmor frequency in an applied magnetic field. In insulators, semiconductors or molecular compounds, on the other hand, the muon will usually pick up one electron and form muonium ($\text{Mu} = \mu^+e^-$) with the size of the Bohr radius and reduced mass and ionization potential very similar to a hydrogen atom [1,2]. Because of the hyperfine coupling of the muon with the electron in Mu, the muon precession frequencies differ significantly from the muon Larmor frequency. This allows us to determine spectroscopically the fraction of muons forming Mu in a sample.

The probability of an implanted μ^+ to form Mu^0 changes in highly defective host materials, as was shown, for example, for neutron-irradiated GaAs [1]. Neutrons with energies of 0.8 to 1.6 MeV and doses up to 8×10^{15} cm^{-3} were used to create antisite defects (As replacing Ga) and Ga-ion vacancies on

the order of 1.5×10^{17} cm^{-3} . After the irradiation, the signal of paramagnetic muonium at the tetrahedral interstitial site (Mu_T^0) remained almost unchanged, while the donorlike bond-centered muonium (Mu_{BC}^0) fraction was transferred to the diamagnetic Mu^+ . Schwab *et al.* concluded that the formation of Mu_{BC}^0 is inhibited by a shortage of electrons (which are trapped by the double-donor antisites), while the low mobility of Mu_T^0 in GaAs permits trapping at the defects. In contrast, early experiments performed on neutron-irradiated Si with defect concentrations up to 2×10^{18} cm^{-3} showed that the Mu_T^0 signal was lost in the damaged samples while the Mu_{BC}^0 signal seemed unaffected [3]. This was explained by assuming that the Mu_T^0 gets dephased by trapping at the defects while the immobile Mu_{BC}^0 is less affected by the radiation damage. Similar results were also reported for electron-irradiated Si samples with doses up to 6×10^{17} cm^{-2} . Again, no Mu_T^0 was formed directly after the irradiation, whereas the Mu_{BC}^0 signal did not change. Upon annealing at higher temperatures, causing a reduction of the irradiation-induced vacancy defects, the Mu_T^0 signal could be recovered [4,5]. Finally, also the extreme case of an amorphous Si host material has been studied and pronounced differences in the Mu formation process compared to poly-crystalline Si were observed [6,7].

So far, most of the μ SR studies on crystal defects in semiconductors, formed either during the growth itself or as a result of irradiation- or implantation-induced lattice damage, were looking at large probing volumes ranging from tens to hundreds of microns. For many device applications, however, optical or electrical properties of the material are modified by actively introducing defects into a shallow region below the surface. In order to control and optimize such processes, methods for the characterization of the thin defective layers are thus required. Low-energy muons (LE- μ^+) with implantation energies below 30 keV provide a valuable extension to

*woerle@aps.ee.ethz.ch

TABLE I. Overview of samples used in this study.

Material	Type	Orientation	Doping N_D (cm^{-3})
Si	<i>n</i> -type	(100)	$\approx 5 \times 10^{11}$
4H-SiC	<i>n</i> -type	(0001)	2.8×10^{15}

conventional bulk μSR techniques, allowing depth-resolved studies of thin films and multilayered structures in the range from a few nm up to ≈ 300 nm [8,9].

Here, we present depth-resolved low-energy μSR (LE- μSR) measurements on proton-irradiated Si and 4H-SiC with irradiation doses ranging from 1×10^{14} to 1×10^{16} cm^{-2} , generating shallow defect profiles near the surface with defect concentrations of up to $\approx 1 \times 10^{19}$ cm^{-3} . By varying the muon energy between 3 and 25 keV, the Mu formation process is studied as function of proton irradiation dose and distance from the semiconductor surface.

II. EXPERIMENTAL DETAILS

For this experiment, two sets of low-doped semiconductor samples, one Si set and one 4H-SiC set, were irradiated with hydrogen (Table I). The implantations were performed at the 350-kV ion implanter at the Ion Technology Centre (ITC), Uppsala University, Uppsala, Sweden. The energy used for the irradiation was 10 keV, resulting in a fairly uniform defect region and a pronounced proton stopping peak located ≈ 130 nm (≈ 100 nm in the case of SiC) below the surface. With a maximal implantation depth of the low-energy muons of about 200 nm, the whole defect profile caused by the proton irradiation can be probed. Three different doses, ranging from 1×10^{14} cm^{-2} to 1×10^{16} cm^{-2} , were chosen for this specific experiment. The lateral defect distribution caused by the proton irradiation is expected to be homogeneous across the 25×25 mm large sample area [10]. After the irradiation, the three 4H-SiC samples were annealed at 1150°C for 3.5h. The proton stopping profiles for Si and 4H-SiC together with the muon stopping ranges are illustrated in Fig. 1. For both sample sets, also a reference sample without a proton irradiation process was analyzed.

Proton-implantation in Si at lower doses is known to produce various defects like vacancy-oxygen (VO) centers, divacancies with several charge states, as well as hydrogen-related centers near the midgap [13,14]. At higher doses, similar to the ones used here, more extended defects such as dislocations, voids, and even amorphous regions are expected [15–17].

For SiC, the high-temperature process will anneal most of the produced point defects apart from the carbon vacancy (V_C) [18–20] and, for high irradiation doses, the divacancy pair $V_{Si}V_C$ [21–23]. A rapid out diffusion of hydrogen during the high-temperature anneal is also expected [24–26]. Considering the different defect creation mechanisms and in comparison with positron-annihilation spectroscopy (PAS) and deep-level-transient spectroscopy studies, a defect density of 1×10^{16} to 1×10^{17} cm^{-3} is assumed for the lowest implantation dose of 1×10^{14} cm^{-2} for Si and 4H-SiC [17,27].

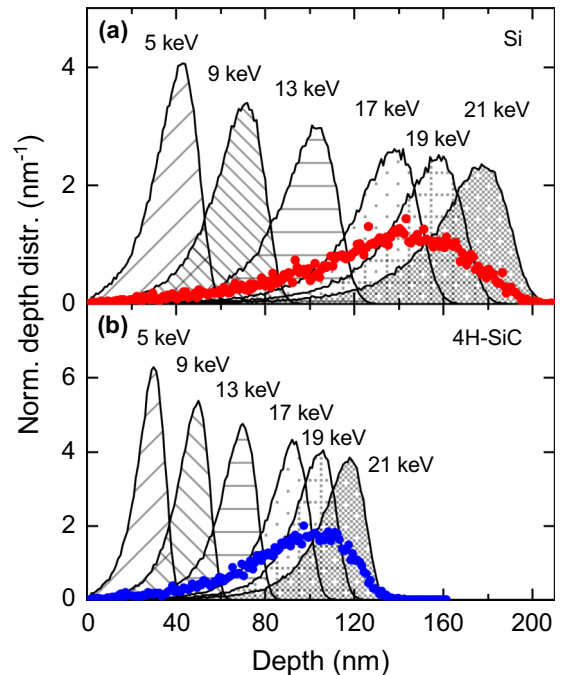


FIG. 1. Muon implantation profiles for energies between 5 and 21 keV (shaded areas) and proton stopping profile (circles), calculated with Trim.SP [11,12] for silicon (a) and silicon carbide (b).

With increasing irradiation dose, the number of defects are assumed to increase more or less linearly as well, yielding a defect density of 1×10^{18} to 1×10^{19} cm^{-3} for the samples with the highest dose. Even with such a high irradiation dose, an amorphization of the semiconductor bulk is not expected [28].

All measurements were performed at the low-energy muon (LEM) beamline at the Swiss Muon Source (S μ S) [9,29]. The samples were glued with silver paste on a Ni-coated Al plate and mounted onto a cryostat placed perpendicular to the muon beam. The final kinetic energy of the μ^+ implanted into the sample was varied between 3 and 24 keV by applying an accelerating or decelerating potential of up to ± 12 keV to the sample. The spot size of the muon beam was 12 mm (FWHM) and the positrons from the muon decay were detected by a set of scintillator detectors placed above, below, left, and right of the beam axis. For all measurements, a magnetic field between 0.5 and 0.15 T was applied parallel to the beam axis normal and transverse to the initial muon spin direction.

III. RESULTS

With μSR , contributions from a diamagnetic (Mu^+ , Mu^-) or paramagnetic (Mu^0) environment can be distinguished. The hyperfine coupling between μ^+ and the electron spin leads to a ≈ 103 times larger muon precession frequency in isotropic Mu at low fields (< 1 mT) compared to the muon Larmor frequency. The dia- and paramagnetic decay asymmetries A_D and A_{Mu} are determined by the amplitudes of the corresponding precession signals and are proportional to the fraction of muons in the particular state. For materials where no Mu^0 is

formed and all μ^+ decay as free muons, the diamagnetic fraction F_D (the ratio of A_D and the total observable asymmetry A_{tot}), is 1. In semiconductors and insulators, smaller values indicate the formation of Mu^0 .

A. Silicon samples

In crystalline silicon, two paramagnetic centers can be distinguished at low temperatures (<150 K): “normal” muonium Mu_T^0 at a tetrahedral interstitial site and the axially symmetric, bond-centered muonium Mu_{BC}^0 . Mu_T^0 has a large isotropic hyperfine coupling of 2006 MHz and the broadened linewidth suggests a trapping of the rapidly diffusing center at intrinsic defects. The isotropy of normal Mu^0 suggests the tetrahedral site with its cubic symmetry as the only possible location inside the crystal. Mu_{BC}^0 , on the other hand, has a smaller, anisotropic coupling of 16.8 MHz (A_{\parallel}) and 92.59 MHz (A_{\perp}), respectively. Here, A_{\parallel} is the coupling constant along the Mu_{BC}^0 symmetry axis, the $\langle 111 \rangle$ bond direction between two Si atoms, and A_{\perp} is the coupling perpendicular to this direction. In low-doped Si crystals and at low temperatures, around 50% of the μ^+ are expected to form Mu_T^0 while roughly 40% will form Mu_{BC}^0 [1].

1. Temperature and doping dependence

With increasing temperature (>130 K), Mu_{BC}^0 is beginning to ionize, resulting in an increased fraction of A_D and hence an increase in F_D . Mu_T^0 , on the other hand, only starts to ionize at temperatures >400 K. Temperature scans from 50 to 160 K performed at three different muon implantation depths, suggesting a partially suppressed Mu^0 formation. The difference between the nonirradiated reference sample and the sample with the lowest irradiation dose ($1 \times 10^{14} \text{ cm}^{-2}$) is minimal, indicating that the Mu formation process is barely affected by the irradiation-induced defect density at this dose. Apart from the $1 \times 10^{16} \text{ cm}^{-2}$ sample, a pronounced increase of F_D appears at higher temperatures, reflecting the thermally induced ionization of Mu_{BC}^0 and its transition to Mu^+ . For the $1 \times 10^{16} \text{ cm}^{-2}$ sample, no Mu_{BC}^0 is formed anymore and F_D is almost temperature independent. A similar behavior has been reported earlier on amorphous Si [7], suggesting that for the sample with the highest proton dose, the crystal is already strongly damaged. Mu_T^0 , on the other hand, should be less defect sensitive; however, at 250 K we still observe a dose dependence of F_D which can only be explained by a transition from Mu_T^0 to Mu^+ triggered by an increased defect concentration.

Figures 2(a) and 2(b) show nearly identical behavior at 5 and 13 keV for each of the four samples suggesting a uniform defect profile for the 100 nm closest to the surface. For a muon energy of 19 keV [Fig. 2(c)], where also the unmodified bulk behind the defective region is partially probed, the change of F_D for different proton doses is less pronounced. Samples with low and medium doses are overlapping with the diamagnetic signal of the nonirradiated sample, while the sample with the highest dose is nearly identical to the diamagnetic signal of the $1 \times 10^{15} \text{ cm}^{-2}$ sample in Figs. 2(a) and 2(b).

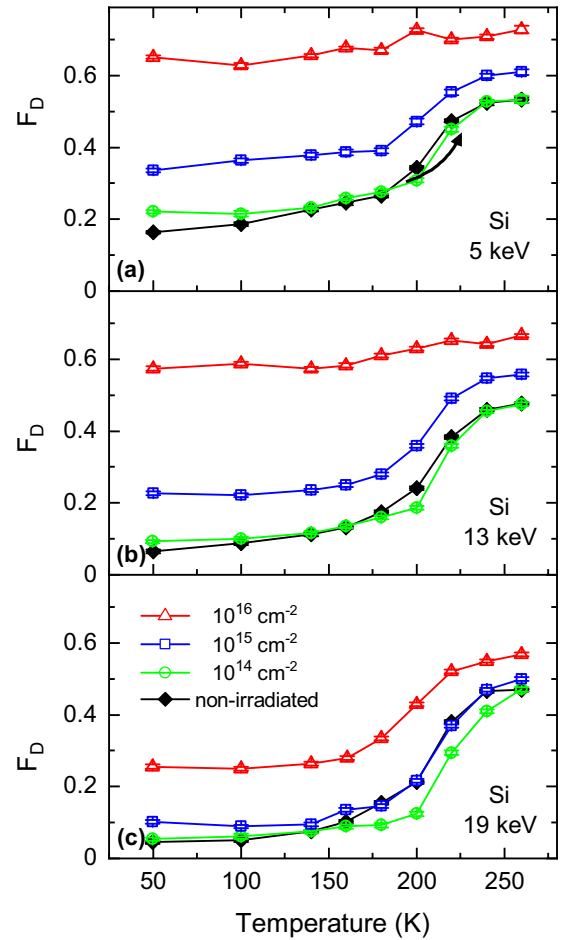


FIG. 2. Temperature scans performed on the Si samples at $B = 10$ mT for three different muon implantation depths. While muons at (a) 5 keV and (b) 13 keV probe only regions within the proton-irradiated region, muons at 19 keV are implanted deep enough to also partially probe the area behind this damaged region (c).

2. Delayed Mu_{BC}^0 formation

In addition to the observed temperature and doping dependence, the formation of Mu_{BC}^0 is also affected by the implantation energy of the muon itself: When the μ^+ is implanted into the material, electron-hole pairs (around 10^3 for the energies used in a LEM experiment [30]) are generated and while some of them quickly recombine, there is a non-negligible probability that some of them may combine with the stopped μ^+ to form Mu_{BC}^0 . For Si and various insulators it was previously shown that Mu_{BC}^0 is formed via this so-called *delayed* formation process and that a sufficiently large amount of excess electrons generated in the ionization track is required [31,32]. (In contrast, Mu_T^0 is formed during slowing down in charge-exchange cycles and a subsequent thermalization of the muonium due to elastic collisions).

The energy scans in Fig. 3(a) illustrate this point more clearly: The decrease of F_D with increasing muon energy reflects the onset of a delayed Mu_{BC}^0 formation with the increasing availability of excess electrons [32]. For a shallow μ^+ implantation depth, the number of e^-h pairs is not sufficient to saturate the Mu_{BC}^0 formation probability, resulting

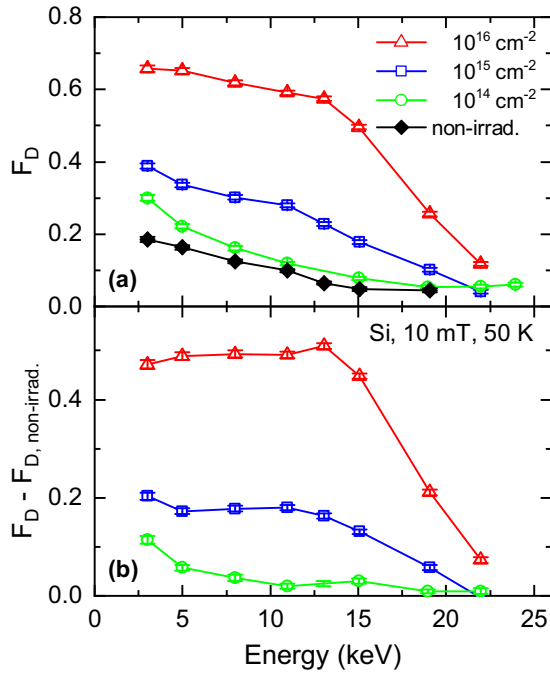


FIG. 3. (a) Diamagnetic fraction of the Si samples as a function of implantation energy for different proton-irradiation doses. $B = 10 \text{ mT}$, $T = 50 \text{ K}$. (b) Change of F_D compared to the nonirradiated sample.

in a larger Mu^+ fraction in the target material and hence an increased value of F_D . It is only at energies $>15 \text{ keV}$ where F_D saturates at its bulk value of ≈ 0.1 . To remove this “surface” effect on the depth dependence of F_D in the irradiated samples, the differences of F_D between the irradiated samples and the reference sample are displayed in Fig. 3(b). For the lowest proton dose, the difference to the nonirradiated Si is minimal, whereas for the two other samples, the diamagnetic signal increases for an increasing defect density. In accordance with the temperature scans in Fig. 2, F_D is almost constant in the region before the implanted H^+ peak, suggesting again a nearly uniform crystal damage in this region. For muon energies $>17 \text{ keV}$ (around 130 nm below the surface), an increasing fraction of the undamaged region behind the end-of-range proton peak is probed and F_D converges to the same low values as for the nonirradiated sample.

3. High- and low-field measurements

In order to study the dia- and paramagnetic decay asymmetries in more detail, additional energy scans at different magnetic fields were acquired. With the limited time resolution and statistics of the setup, only Mu precession frequencies $<60 \text{ MHz}$ can be resolved, which is sufficient for a direct observation of the Mu_{BC}^0 transitions at an applied field of 0.15 T. The transition frequencies between the triplet states of Mu_T^0 at this field, however, are too high to be resolved with the experimental time resolution of about 10 ns FWHM, and a low field of 0.5 mT is used to observe the Mu_T^0 precession frequency. (Note that at this low field, the Mu_{BC}^0 transitions frequencies are too heavily damped to be observed [32]). Figures 4(a) and 4(b) show A_D and A_{MuBC} measured at

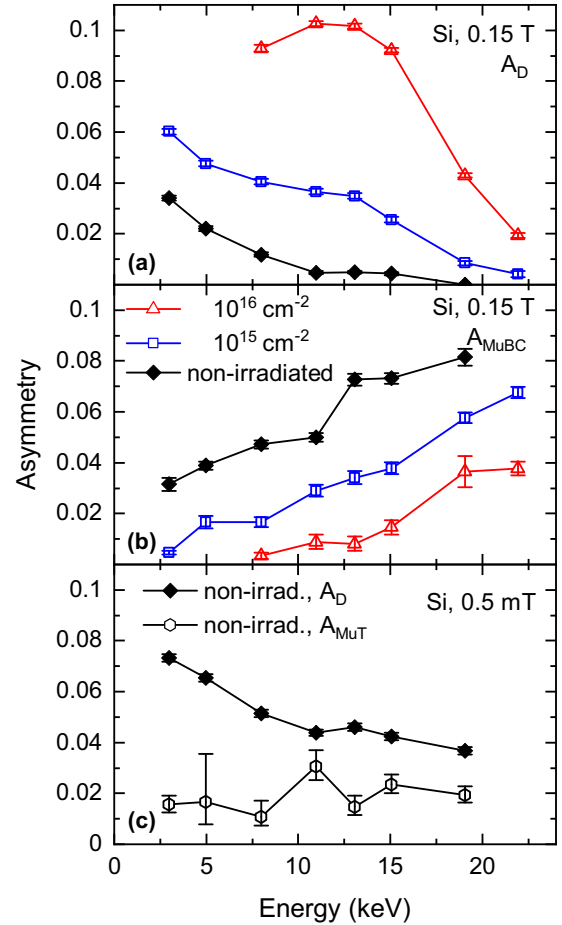


FIG. 4. (a) Diamagnetic and (b) Mu_{BC}^0 asymmetries as a function of the muon implantation energy for the nonirradiated and two proton-irradiated Si samples with doses of $1 \times 10^{15} \text{ cm}^{-2}$ and $1 \times 10^{16} \text{ cm}^{-2}$, taken at $B = 0.15 \text{ T}$. (c) Low-field measurement of A_D and A_{MuT} for the nonirradiated Si sample with $B = 0.5 \text{ mT}$. All measurements were performed at $T = 50 \text{ K}$.

$B = 0.15 \text{ T}$ and $T = 50 \text{ K}$ for two proton-irradiated samples and the nonirradiated reference. While for the nonirradiated and the medium-dose sample, the change of A_D can be explained by a proportional increase of A_{MuBC} , the sample with the highest proton dose ($1 \times 10^{16} \text{ cm}^{-2}$) exhibits a significantly increased diamagnetic asymmetry with only slightly reduced A_{MuBC} values. This discrepancy can be explained by a suppression of Mu_T^0 formation in the highly defective region ($<130 \text{ nm}$) which was also observed in the temperature scans in Figs. 2(a) and 2(b). Measurements performed at low magnetic field ($B = 0.5 \text{ mT}$) revealed a strongly damped Mu_T^0 signal and A_{MuT} could only be measured for the nonirradiated sample [Fig. 4(c)]. The reason for larger A_D values obtained in the low-field measurements in Fig. 4(c) compared to the analysis at high field [Fig. 4(a)] is the finite time resolution of the LEM setup, causing a reduction of the observable asymmetry at 0.15 T to about 60% of its value at 0.5 mT [Fig. 4(c)].

B. 4H-SiC samples

The results obtained for 4H-SiC show similarities with the measurements performed on Si, even though the Mu

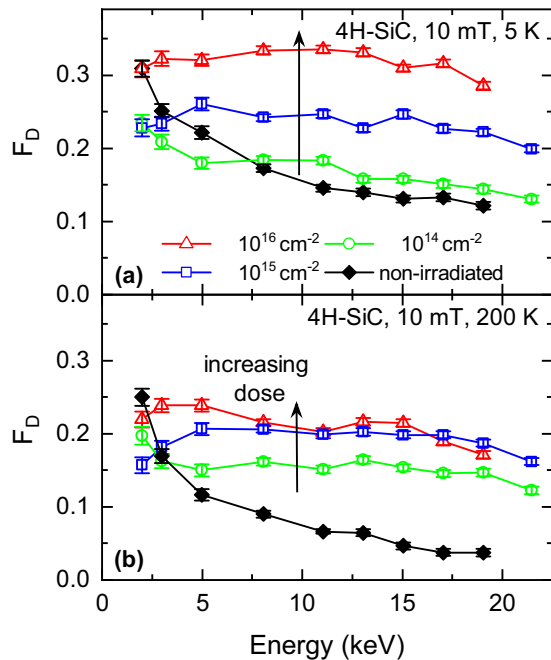


FIG. 5. Diamagnetic fraction of the 4H-SiC samples, taken at 10 mT and two different temperatures: (a) 5 K and (b) 200 K.

formation is quite different for the two semiconductors. In 4H-SiC, also two paramagnetic centers are observed, commonly referred to as Mu_1^0 and Mu_2^0 . Unlike Si, however, there is no evidence of a bond-centered Mu^0 state with small and highly anisotropic hyperfine interactions and Mu_1^0 and Mu_2^0 show both relatively large and almost isotropic hyperfine characteristics. Lichti *et al.* assign Mu_1^0 with its acceptor-like properties to locations with tetrahedral local symmetry and Si as nearest neighbors [33]. For the donor-like Mu_2^0 , either an antibonding to a carbon atom (AB_C) or a Si atom (AB_{Si}) are suggested [34].

Energy scans for all four 4H-SiC samples measured at 5 and 200 K are presented in Fig. 5. Again, an increase in F_D —at the expense of Mu^0 —is clearly observable for increasing defect densities. For muon energies >15 keV, the diamagnetic fraction slowly drops for all proton-irradiated samples, indicating the transition to the nondamaged crystal behind the irradiated region.

Unlike suggested in earlier studies on *n*-type 4H-SiC [33–35], almost no temperature dependence is observed for SiC in this temperature range and the energy scans in Fig. 5 are very similar despite the temperature difference of almost 200 K. This discrepancy appears to be related to the considerably lower doping level of our 4H-SiC samples ($N_D = 2.8 \times 10^{15} \text{ cm}^{-3}$) compared to previous studies on 4H-SiC samples, resulting in an inefficient transition from neutral Mu^0 to diamagnetic Mu^- and hence a reduced temperature dependence.

As discussed above for Si, Mu_{BC}^0 is only formed when the muons are implanted with a sufficiently high energy of several keV. For 4H-SiC on the other hand, such a delayed Mu^0 formation process has not been reported so far and as expected, F_D in Fig. 5 is nearly constant at shallow probing depths for the proton-irradiated samples. In the case of the

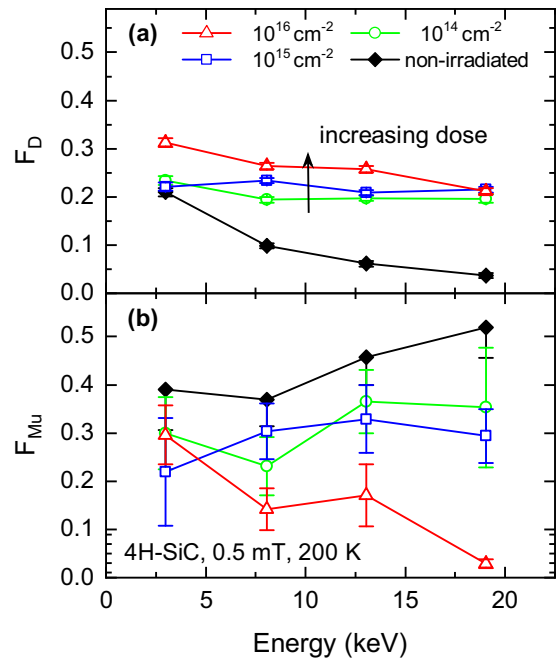


FIG. 6. (a) Diamagnetic and (b) Mu fractions of the 4H-SiC samples, measured at 0.5 mT and 200 K. A stronger transition of Mu_7^0 to Mu^+ for increasing defect densities is again observed. The missing fraction is around 40%.

reference sample, however, a pronounced increase of F_D for the first few keV is observed, suggesting either an increased defect concentration close to the surface or a delayed Mu formation. Since all four samples were cut from the same wafer and processed in parallel, a surface contamination or an inhomogeneous doping of the epitaxy in the reference sample seems unlikely. Another difference is that the nonirradiated sample did not undergo a high-temperature annealing step, though we do not expect that this could explain the differences of F_D at low muon implantation depths.

A delayed Mu^0 formation is therefore the most likely mechanism to explain the observed energy dependence. This assumption is further supported by the asymmetry data of the reference sample in Fig. 6. As expected for delayed Mu^0 formation, an increasing diamagnetic signal [Fig. 6(a)] when lowering the implantation energy below ≈ 15 keV is observed, while the Mu^0 asymmetry A_{Mu} is decreasing [Fig. 6(b)]. In the proton-irradiated samples, both F_D and A_{Mu} are almost constant as a function of energy, and no transfer from Mu^0 to Mu^+ is observed.

In addition, there are clear indications of a delayed formation of the diamagnetic signal in the proton-irradiated 4H-SiC samples. In the low-field measurements at 0.5 mT and 200 K [Fig. 6(a)], the diamagnetic fraction of the nonirradiated sample is about the same as the results at 10 mT. In contrast, F_D of the proton-irradiated samples is reduced at 10 mT and 200 K [Fig. 5(a)]. This field dependence indicates the presence of a neutral precursor state which transforms within a time shorter than the neutral precursor hyperfine period into a diamagnetic state. With increasing magnetic field, the muon spins in the neutral precursor state lose the phase coherence, resulting in a decrease of observable diamagnetic fraction [34,36].

Interestingly, at 5 K the diamagnetic fractions of the 10^{14} and 10^{15} cm^{-2} samples are larger compared to 200 K, indicating a faster transfer of the neutral precursor to the diamagnetic state at lower temperature.

IV. DISCUSSION

A. Comparison to other techniques

Besides theoretical calculations, there exist a variety of experimental methods for the investigation of defects and crystal damage in semiconductors and all of them come with their own benefits and limitations. Electrical and optical defect spectroscopy can give valuable information on basic semiconductor properties such as resistivity, carrier mobility, or optical transitions between the valence and conduction bands. A widely employed technique is deep-level transient spectroscopy (DLTS), which can be used for moderate defect concentrations in the range of $N_{\text{defect}}/N_D < 10^{-4}$ [37]. DLTS also allows for a depth-resolved analysis although probing very thin layers, especially close to the surface as in the samples investigated here, may prove unreliable. Magnetic resonance techniques such as electron spin resonance (ESR) are often employed to study the total number of active centers in a semiconductor. One limitation of ESR is that only paramagnetic ionized states can be probed and difficulties arise again in the case of thin films and highly doped materials. There also exist a variety of particle beam methods which use ion beams for the acquisition of defect profiles. Although most of them are destructive techniques, there also exist some non-destructive methods such as Rutherford backscattering spectrometry [38] or positron annihilation spectroscopy (PAS). The latter is sensitive to vacancy-like defect concentrations in the range from 10^{15} to 10^{19} cm^{-3} [39]. By varying the energy of a slow positron beam, defect profiles up to a few microns depth can be extracted. While low-energy PAS works well for defective regions close to the surface, the positron implantation profile broadens with increasing positron energy and its FWHM quickly becomes comparable to the mean implantation depth [40].

LE- μ SR is particularly attractive for its high depth resolution and the ability to also probe thin layers close to the sample surface. In terms of the technique's sensitivity to point defects, our experimental results suggest slightly different limits for Si and 4H-SiC: While hardly any change in the μ SR signal was observed for the Si sample with the lowest proton irradiation dose, we already see a pronounced effect in the case of 4H-SiC. From the TrimSP simulations of the investigated samples, a defect concentration of around $1 \times 10^{18} \text{ cm}^{-3}$ was derived for the lowest proton irradiation dose assuming that every proton generates between 2.5 and 5 vacancies per 10 keV proton and only around 5% survived dynamic annealing [18]. Similar defect densities were also reported in PAS studies on proton- or electron-irradiated Si and 4H-SiC, where defect concentrations between 5×10^{16} and $1 \times 10^{20} \text{ cm}^{-3}$ for implantation doses ranging from 1×10^{14} to $1 \times 10^{16} \text{ cm}^{-3}$ were measured [17,24,26,41,42]. Therefore, we estimate a lower sensitivity limit of about 10^{17} to 10^{18} cm^{-3} for Si although the strong temperature and field dependence of the Mu signal in 4H-SiC may allow to probe even lower defect densities. Compared to DLTS or PAS,

this sensitivity is at least two orders of magnitude higher; nevertheless, the ability to also probe strongly damaged as well as very thin semiconductor layers makes LE- μ SR an appealing complementary analysis tool.

B. Damage profiles as detected by μ SR

Both for Si and 4H-SiC, the concentration of defects which modify the Mu formation process is almost constant until the μ^+ reach approximately the peak position of the stopping distribution; from this depth on, the diamagnetic fraction seems to quickly recover to the bulk value, implying a rapid drop of the defect concentration after the peak. This is in accordance with SRIM simulations [43], where a uniform vacancy distribution before the H^+ stopping peak was extracted.

C. Delayed Mu formation

Finally, we want to comment the formation of delayed Mu in the presence of different defect levels: In Si and insulators, excess electrons from the ionization track at a distance of 50–100 nm to the stopped muon can contribute to the delayed Mu formation [31,32]. We begin to observe a reduction of delayed Mu formation at a defect concentration of about $1 \times 10^{18} \text{ cm}^{-3}$, corresponding to a mean distance between defects of 10 nm. This implies that at this average distance of defects, the excess electrons from the ionization track are likely to be trapped at one of the defects before being captured by the positive muon. Larger distances between defects, i.e., lower defect concentrations, do not seem to affect the delayed muonium formation process. For 4H-SiC, a delayed Mu formation is only observed for the nonirradiated sample.

V. CONCLUSIONS

In conclusion, the potential of LE- μ^+ SR for a depth-resolved analysis of defect profiles in semiconductors was successfully demonstrated. For both materials studied in this work, it was shown that the changes of diamagnetic fractions could be explained by a suppression of Mu formation and that this trend was more pronounced for increasing proton irradiation densities. A nearly uniform damage profile for the entire proton-irradiated region without a pronounced sensitivity to the proton stopping peak at the end of the irradiation range was observed. In the case of the annealed 4H-SiC samples, the dose-dependent variations in F_D may be directly linked to the V_C concentration in the material.

Despite a rather low estimated sensitivity for crystal defects of about 10^{17} to 10^{18} cm^{-3} , the possibility of a nondestructive probing of near-surface regions without the need of fabricating an electronic device can give valuable complementary information when investigating defects in semiconductors.

ACKNOWLEDGMENTS

The muon measurements have been performed at the Swiss Muon Source ($S\mu S$), Paul Scherrer Institute, Villigen, Switzerland. The Ion Technology Centre (ITC) at Uppsala University, Sweden, is acknowledged for the proton implantations.

- [1] B. D. Patterson, *Rev. Mod. Phys.* **60**, 69 (1988).
- [2] A. Yaouanc and P. D. de Réotier, *Muon Spin Rotation, Relaxation, and Resonance: Applications to Condensed Matter* (Oxford University Press, Oxford, UK, 2011).
- [3] S. G. Barsov, A. L. Getalov, V. A. Gordeev, V. A. Evseev, R. F. Konopleva, S. P. Kruglov, V. I. Kudinov, L. A. Kuz'min, S. M. Mikirtychants, E. V. Minaichev, G. G. Myasishcheva, Y. V. Obukhov, G. I. Savel'ev, V. G. Firsov, and G. V. Shcherbakov, *Hyperfine Interact.* **18**, 551 (1984).
- [4] E. Albert, S. Barth, A. Möslang, E. Recknagel, A. Weidinger, and P. Moser, *Appl. Phys. Lett.* **46**, 759 (1985).
- [5] E. Westhauser, E. Albert, M. Hamma, E. Recknagel, A. Weidinger, and P. Moser, *Hyperfine Interact.* **32**, 589 (1986).
- [6] A. Singh, *J. Mater. Sci.* **31**, 1991 (1996).
- [7] E. A. Davis, A. Singh, S. F. J. Cox, S. R. Kreizman, T. L. Estle, B. Hitti, R. L. Lichti, D. Lamp, R. Duvarney, D. W. Cooke, M. Paciotti, and A. C. Wright, *J. Non-Cryst. Solids* **137–138**, 17 (1991).
- [8] E. Morenzoni, T. Prokscha, A. Suter, H. Luetkens, and R. Khasanov, *J. Phys.: Condens. Matter* **16**, 4583 (2004).
- [9] T. Prokscha, E. Morenzoni, K. Deiters, F. Foroughi, D. George, R. Kobler, A. Suter, and V. Vrankovic, *Nucl. Instrum. Methods Phys. Res., Sect. A* **595**, 317 (2008).
- [10] A. Hallén, P. A. Ingemarsson, P. Håkansson, B. U. R. Sundqvist, and G. Possnert, *Nucl. Instrum. Methods Phys. Res., Sect. B* **36**, 345 (1989).
- [11] W. Eckstein, *Computer Simulation of Ion-Solid Interactions*, Springer Series in Materials Science (Springer, Berlin, 1991).
- [12] E. Morenzoni, H. Glückler, T. Prokscha, R. Khasanov, H. Luetkens, M. Birke, E. M. Forgan, C. Niedermayer, and M. Pleines, *Nucl. Instrum. Methods Phys. Res., Sect. B* **192**, 254 (2002).
- [13] A. Hallén, B. U. R. Sundqvist, Z. Paska, B. G. Svensson, M. Rosling, and J. Tirén, *J. Appl. Phys.* **67**, 1266 (1990).
- [14] P. Lévêque, P. Pellegrino, A. Hallén, B. G. Svensson, and V. Privitera, *Nucl. Instrum. Methods Phys. Res., Sect. B* **174**, 297 (2001).
- [15] S. Kirnstoetter, M. Faccinelli, C. Gspan, W. Grogger, M. Jelinek, W. Schustereder, J. G. Laven, H.-J. Schulze, and P. Hadley, *Phys. Stat. Solidi C* **11**, 1545 (2014).
- [16] M. Jelinek, J. Laven, M. Rommel, W. Schustereder, H.-J. Schulze, L. Frey, and R. Job, *ECS Trans.* **64**, 173 (2014).
- [17] M. A. Lourenço, A. P. Knights, K. P. Homewood, R. M. Gwilliam, P. J. Simpson, and P. Mascher, *Nucl. Instrum. Methods Phys. Res., Sect. B* **175–177**, 300 (2001).
- [18] A. Hallén, M. S. Jansson, A. Y. Kuznetsov, D. Åberg, M. K. Linnarsson, B. G. Svensson, P. O. Persson, F. H. C. Carlsson, L. Storasta, J. P. Bergman, S. G. Sridhara, and Y. Zhang, *Nucl. Instrum. Methods Phys. Res., Sect. B* **186**, 186 (2002).
- [19] G. Alfieri, E. V. Monakhov, B. G. Svensson, and A. Hallén, *J. Appl. Phys.* **98**, 113524 (2005).
- [20] H. M. Ayedh, A. Hallén, and B. G. Svensson, *J. Appl. Phys.* **118**, 175701 (2015).
- [21] C. C. Ling, C. D. Beling, and S. Fung, *Phys. Rev. B* **62**, 8016 (2000).
- [22] W. E. Carlos, N. Y. Garces, E. R. Glaser, and M. A. Fanton, *Phys. Rev. B* **74**, 235201 (2006).
- [23] N. T. Son, P. Carlsson, J. ul Hassan, B. Magnusson, and E. Janzén, *Phys. Rev. B* **75**, 155204 (2007).
- [24] M. Janson, M. K. Linnarsson, A. Hallén, and B. G. Svensson, *MRS Proc.* **513**, 439 (1998).
- [25] P. Deák, A. Gali, and B. Aradi, Hydrogen in SiC, in *Silicon Carbide*, edited by W. J. Choyke, H. Matsunami, and G. Pensl (Springer, Berlin, 2004), Chap. 3, pp. 57–88.
- [26] A. Barcz, M. Kozubal, R. Jakiela, J. Ratajczak, J. Dyczewski, K. Gołaszewska, T. Wojciechowski, and G. K. Celler, *J. Appl. Phys.* **115**, 223710 (2014).
- [27] L. Storasta, F. H. C. Carlsson, S. G. Sridhara, B. Formanek, P. Bergman, A. Hallén, and E. Janzén, *Mater. Sci. Forum* **353–356**, 431 (2001).
- [28] W. Puff, A. G. Balogh, and P. Mascher, *Mater. Sci. Forum* **338–342**, 965 (2000).
- [29] E. Morenzoni, H. Glückler, T. Prokscha, H. P. Weber, E. M. Forgan, T. J. Jackson, H. Luetkens, C. Niedermayer, M. Pleines, M. Birke, A. Hofer, J. Litterst, T. Riseman, and G. Schatz, *Phys. B: Condens. Matter* **289–290**, 653 (2000).
- [30] F. E. Emery and T. A. Rabson, *Phys. Rev.* **140**, A2089 (1965).
- [31] D. G. Eshchenko, V. G. Storchak, J. H. Brewer, G. D. Morris, S. P. Cottrell, and S. F. J. Cox, *Phys. Rev. B* **66**, 035105 (2002).
- [32] T. Prokscha, E. Morenzoni, D. G. Eshchenko, N. Garifianov, H. Glückler, R. Khasanov, H. Luetkens, and A. Suter, *Phys. Rev. Lett.* **98**, 227401 (2007).
- [33] R. L. Lichti, W. A. Nussbaum, and K. H. Chow, *Phys. Rev. B* **70**, 165204 (2004).
- [34] Y. G. Celebi, R. L. Lichti, H. N. Bani-Salameh, A. G. Meyer, B. R. Carroll, J. E. Vernon, P. J. C. King, and S. F. J. Cox, *Phys. B: Condens. Matter* **404**, 845 (2008).
- [35] Y. G. Celebi, R. L. Lichti, B. R. Carroll, P. J. C. King, and S. F. J. Cox, *Phys. B: Condens. Matter* **404**, 5117 (2009).
- [36] T. Prokscha, *Phys. Procedia* **30**, 50 (2012).
- [37] D. K. Schroder, *Semiconductor Material and Device Characterization* (John Wiley & Sons, New York, 2005).
- [38] Y. Zhang, A. Debelle, A. Boulle, P. Kluth, and F. Tuomisto, *Curr. Opin. Solid State Mater. Sci.* **19**, 19 (2015).
- [39] F. Tuomisto and I. Makkonen, *Rev. Mod. Phys.* **85**, 1583 (2013).
- [40] M. Fujinami, T. Miyagoe, T. Sawada, and T. Akahane, *J. Appl. Phys.* **94**, 4382 (2003).
- [41] A. A. Lebedev, A. I. Veinger, D. V. Davydov, V. V. Kozlovski, N. S. Savkina, and A. M. Strel'chuk, *J. Appl. Phys.* **88**, 6265 (2000).
- [42] L. Henry, M.-F. Barthe, C. Corbel, P. Desgardin, G. Blondiaux, S. Arpiainen, and L. Liskay, *Phys. Rev. B* **67**, 115210 (2003).
- [43] J. F. Ziegler, M. D. Ziegler, and J. P. Biersack, *Nucl. Instrum. Methods Phys. Res., Sect. B* **268**, 1818 (2010).